iScience

CellPress

Article

Safety of Whole-Body Abrogation of the TRF1 Shelterin Protein in Wild-Type and Cancer-Prone Mouse Models

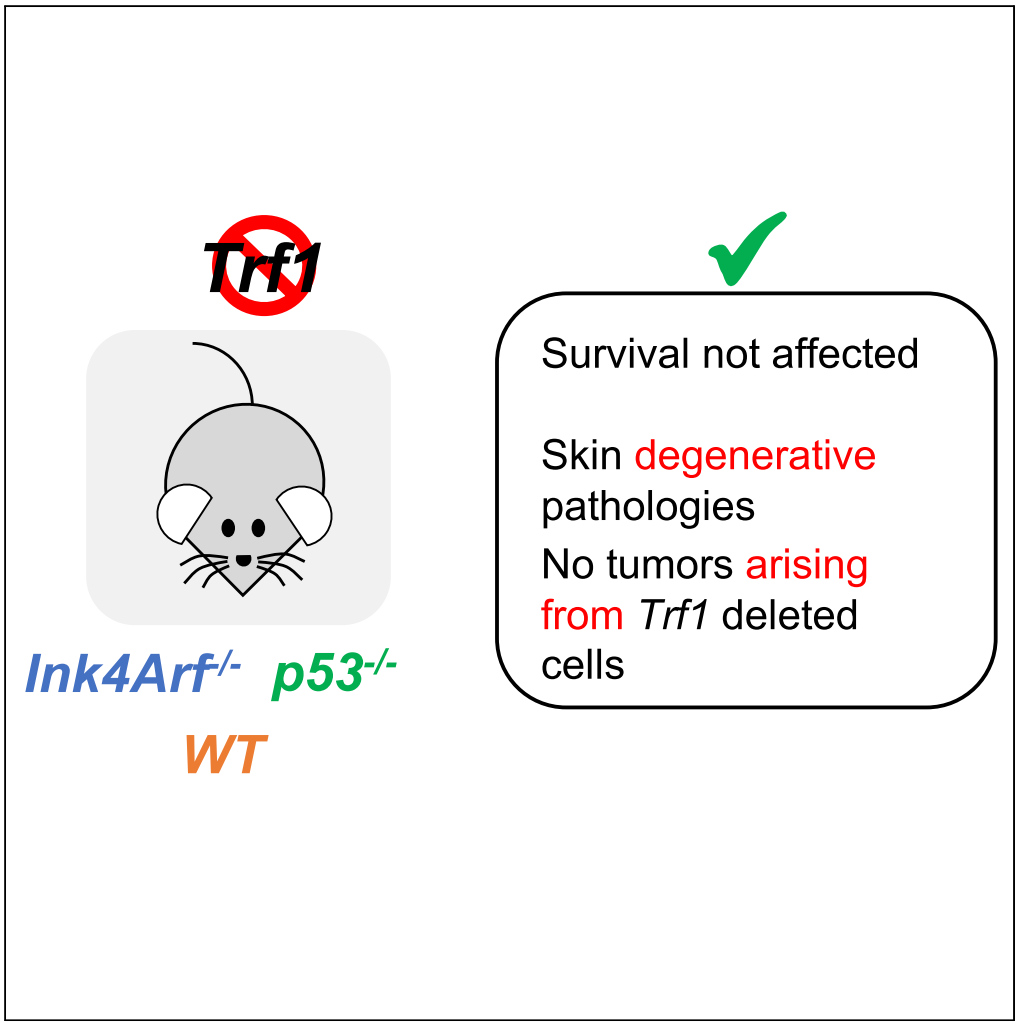

Leire Bejarano, Jessica Louzame, Juán José Montero, Diego Megías, Juana M. Flores, Maria A. Blasco

mblasco@cnio.es

HIGHLIGHTS

Trf1 deletion does not affect organism viability in WT and cancer-prone mouse models

Trf1 deletion only induces mild phenotypes in adult tissues, especially in the skin

No tumors originate from *Trf1*-deleted cells

Bejarano et al., iScience *19*, 572–585
September 27, 2019
https://doi.org/10.1016/j.isci.2019.08.012

iScience

CellPress

Article

Safety of Whole-Body Abrogation of the TRF1 Shelterin Protein in Wild-Type and Cancer-Prone Mouse Models

Leire Bejarano,[1] Jessica Louzame,[1] Juán José Montero,[1] Diego Megías,[2] Juana M. Flores,[3] and Maria A. Blasco[1,4,*]

SUMMARY

Telomeres are considered potential anti-cancer targets. Most studies have focused on telomerase inhibition, but this strategy has largely failed in clinical trials. Direct disruption of the shelterin complex through TRF1 inhibition can block tumorigenesis in cancer mouse models by a mechanism that involves DNA damage induction and reduction of proliferation and stemness. Any anti-cancer target, however, must fulfill the requisite of not showing deleterious effects in healthy tissues. Here, we show that *Trf1* genetic deletion in wild-type and cancer-prone *p53*- and *Ink4Arf*-deficient mice does not affect organismal viability and only induces mild phenotypes like decreased body weight and hair graying or hair loss, the skin being the most affected tissue. Importantly, we found that *Trf1* is essential for tumorigenesis in *p53*- and *Ink4Arf*-deficient mice, as we did not find a single tumor originating from *Trf1*-deleted cells. These findings indicate a therapeutic window for targeting *Trf1* in cancer treatment.

INTRODUCTION

Telomeres are heterochromatic structures at the ends of chromosomes that consist of tandem repeats of the TTAGGG sequence bound by a protective six-protein complex known as shelterin (Liu et al., 2004). Shelterin encompasses TRF1, TRF2, RAP1, TPP1, TIN2, and POT1, and all of them, except for RAP1, are essential for telomere protection (De Lange, 2005; Martinez et al., 2010). In particular, shelterin-bound telomeres protect chromosome ends from degradation and repair activities in this manner preventing end-to-end chromosome fusions and ensuring chromosome stability (De Lange, 2005). Telomeres shorten throughout the lifespan of organisms associated to cell division owing to the so-called end replication problem, eventually jeopardizing tissue regeneration and organismal viability (Harley et al., 1990). Telomere shortening can be compensated through *de novo* addition of telomeric repeats by telomerase, a reverse transcriptase composed of a catalytic subunit (TERT) and an RNA component (Terc), which is used as template for the synthesis of telomeric repeats (Greider and Blackburn, 1985). Telomerase is highly active in pluripotent stem cells during embryonic development; however, it is silenced in the majority of differentiated cells after birth, thus leading to telomere shortening with aging (Martínez and Blasco, 2011). Telomeres can also be elongated by an alternative mechanism known as alternative lengthening of telomeres (ALT), which is based on homologous recombination (Bryan et al., 1997).

Telomeres are considered as potential anti-cancer targets (Hanahan and Weinberg, 2011). Cancer cells are known for their high proliferation rate, which induces a rapid telomere shortening followed by activation of DNA damage response (DDR) pathways that can lead to apoptosis or senescence. Any neoplastic cell should overcome these barriers to achieve an unlimited replicative potential, which in turn relies on telomere maintenance mechanisms (Hanahan and Weinberg, 2011). In fact, more than 90% human tumors aberrantly over-express telomerase (Kim et al., 1994; Shay and Bacchetti, 1997), whereas the remaining telomerase-negative tumors activate ALT (Bryan et al., 1997; Barthel et al., 2017).

Most studies aiming to target telomeres in cancer have focused on telomerase inhibition as therapeutic approach to prevent telomere elongation in cancer cells (Harley, 2008). Indeed, telomerase is heavily mutated in many different cancer types, and telomerase activation is seen in 90%–95% of all tumor types (Kim et al., 1994; Shay and Bacchetti, 1997; Joseph et al., 2010).The most advanced anti-telomerase drug is GRN163L, also called imetelstat (Harley, 2008). However, both mouse models and human clinical

[1]Telomeres and Telomerase Group, Molecular Oncology Program, Spanish National Cancer Centre (CNIO), Melchor Fernández Almagro 3, Madrid 28029, Spain

[2]Confocal Microscopy Unit, Biotechnology Program, Spanish National Cancer Research Centre (CNIO), Madrid 28029, Spain

[3]Animal Surgery and Medicine Department, Faculty of Veterinary Science, Complutense University of Madrid, Madrid, Spain

[4]Lead Contact

*Correspondence: mblasco@cnio.es

https://doi.org/10.1016/j.isci.2019.08.012

trials have shown the limitations of this strategy, as the anti-tumorigenic effect is only achieved when telomeres reach a critically short length (Gonzalez-Suarez et al., 2000; Perera et al., 2008) and this effect is lost in the absence of the *p53* tumor suppressor gene, which is frequently mutated in cancer. In addition, telomerase inhibition may favor the activation of alternative telomere elongation mechanisms based on recombination as extensively shown in yeast and mammalian cells (Bryan et al., 1997; Barthel et al., 2017).

Interestingly, not only telomerase but also shelterins are mutated in cancer. In this regard, we and others have found that POT1 is mutated in several types of sporadic and familial human cancers, including chronic lymphocytic leukemia (Ramsay et al., 2013), familial melanoma (Robles-Espinoza et al., 2014; Shi et al., 2014), Li-Fraumeni-like families with cardiac angiosarcomas (Calvete et al., 2015), glioma (Bainbridge et al., 2015), mantle cell lymphoma (Zhang et al., 2014), and parathyroid adenoma (Newey et al., 2012). These studies highlight the possibility of targeting the shelterin complex as a novel and promising strategy to target telomeres in cancer, which would lead to a rapid telomere dysfunction independently of telomere length, thus avoiding the shortcomings of telomerase inhibition. Indeed, several studies demonstrate that TRF1 inhibition could represent an alternative to telomerase to target telomeres more efficiently. TRF1 directly binds TTAGGG telomeric DNA where it is essential for telomere protection (De Lange, 2005; Martínez and Blasco, 2011). *Trf1* genetic deletion *in vivo* induces a persistent DDR at telomeres, which is sufficient to block cell division and induce apoptosis or senescence in several mouse tissues, independently of telomere length (Martínez et al., 2009; Beier et al., 2012; Schneider et al., 2013; Povedano et al., 2015). Interestingly, TRF1 is over-expressed in adult stem cell compartments and in pluripotent stem cells, where it is essential to maintain tissue homeostasis and pluripotency, respectively (Boué et al., 2010; Schneider et al., 2013). Over-expression of TRF1 has been also reported in several types of cancers such as renal cell carcinoma (Pal et al., 2015) and gastrointestinal tumors (Hu et al., 2010). Furthermore, we have recently reported that induction of telomere uncapping by *Trf1* genetic depletion or chemical inhibition can effectively block the growth of very aggressive and rapidly growing lung tumors in *p53*-deficient *K-RasG12V* mice, in a manner that is independent of telomere length (García-Beccaria et al., 2015), thus further supporting that TRF1 could be a good anti-cancer target for aggressive tumors. We recently validated this hypothesis using glioblastoma (GBM) mouse models in which we demonstrated that *Trf1* deletion blocks both tumor initiation and progression, showing great impact on mice survival (Bejarano et al., 2017).

Given the promising results of TRF1 inhibition in two independent tumors types (i.e., lung cancer and glioblastoma), in the present work we aim to study the safety of long-term *Trf1* genetic deletion in wild-type (WT) and cancer-prone mouse models.

RESULTS

Whole-Body *Trf1* Deletion Does Not Affect Mouse Survival in the Context of Wild-Type or Cancer-Prone Mouse Models

Any potential anti-cancer target must fulfill the important requisite of not showing deleterious effects in healthy tissues or compromising organism viability. In line with this, we previously demonstrated that *Trf1* whole-body deletion in adult mice does not impair organismal viability over a 6-month follow-up period and only leads to mild loss of cellularity in highly proliferative tissues (García-Beccaria et al., 2015; Bejarano et al., 2017). However, potential lifelong adverse effects of *Trf1* deletion in a healthy organism are still unknown. In addition, the long-term effects of *Trf1* deletion and the associated telomere damage in cancer-prone mouse models are unknown. Thus, here we set to study the long-term effects of *Trf1* whole-body deletion in three independent genetic backgrounds, including both WT and cancer-prone *Ink4Arf*$^{-/-}$ and *p53*$^{-/-}$ backgrounds. To this end, we took advantage of the *Trf1*-inducible knockout mice previously described by us (Martínez et al., 2009) to generate the following independent mouse cohorts, which allow for *Trf1* deletion upon tamoxifen administration in the diet: *Trf1*$^{lox/lox}$ or *Trf1*$^{+/+}$, hUBC-CreERT2, *Ink4Arf*$^{-/-}$ mice; *Trf1*$^{lox/lox}$ *or Trf1*$^{+/+}$, hUBC-CreERT2, *p53*$^{-/-}$ mice; and *Trf1*$^{lox/lox}$ or *Trf1*$^{+/+}$, hUBC-CreERT2 mice. Next, we induced *Trf1* deletion by administering tamoxifen in the diet at 6 weeks of age in the case of *p53*$^{-/-}$ mice and at 10 weeks of age in the case of the *Ink4rf*$^{-/-}$ and WT cohorts (Figure 1A). The tamoxifen diet was started earlier in the case of *p53*$^{-/-}$ mice owing to their shorter lifespan due to earlier tumor development (Jacks et al., 1994). In all cases, the tamoxifen diet was maintained until the humane endpoint. At this time point (humane endpoint), we determined TRF1 levels in different mouse tissues by using immunofluorescence (Methods). In all genetic backgrounds, we observed that *Trf1*$^{lox/lox}$ mice showed decreased TRF1 nuclear fluorescence foci in all the organs studied compared with control *Trf1*$^{+/+}$ mice (Figures 1B–1D). In addition, we confirmed *Trf1* deletion by performing qRT-PCR (Figures

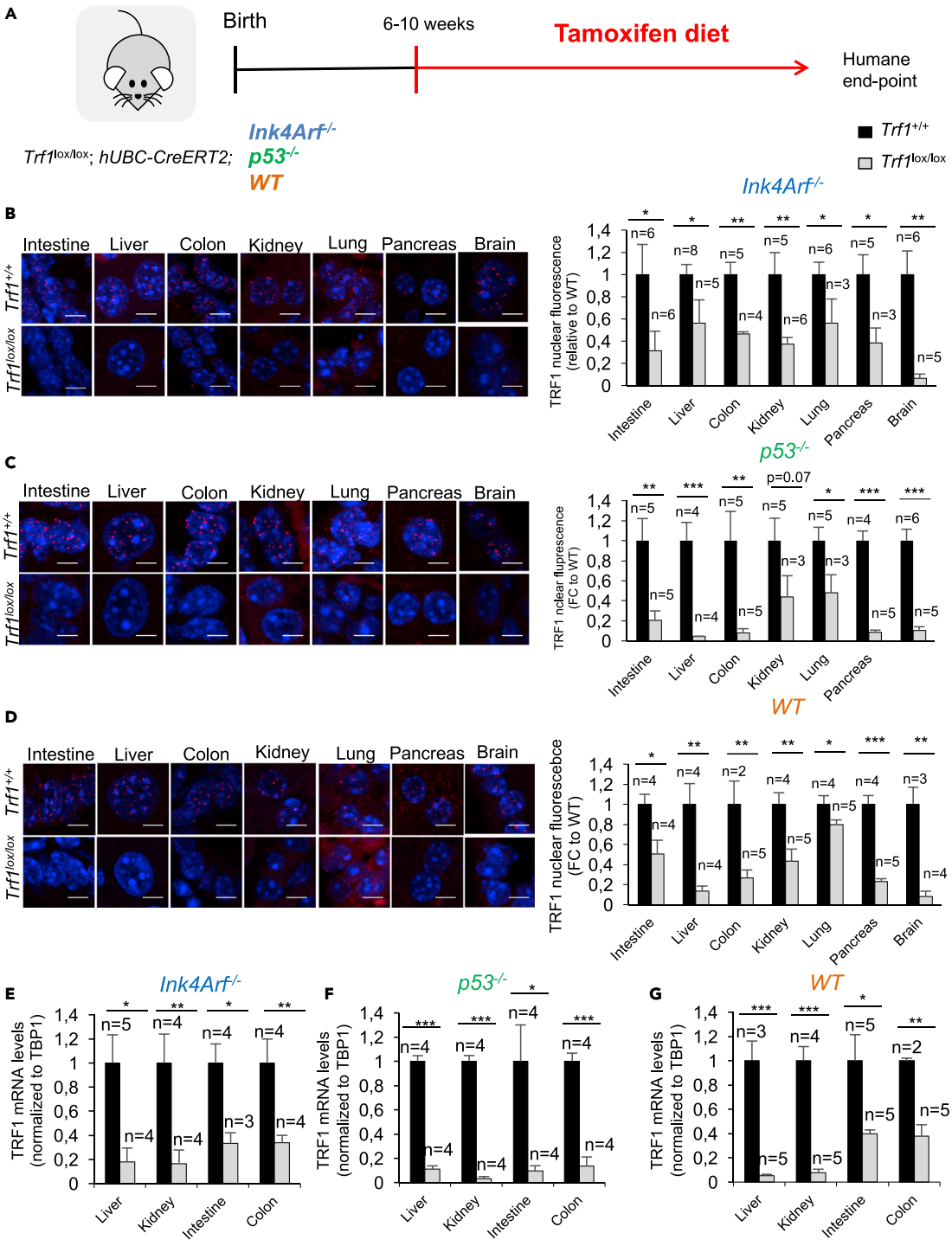

Figure 1. Analysis of *Trf1* Deletion in Multiple Organs

(A) The different mouse cohorts started tamoxifen treatment at 6–10 weeks' age. Mice were sacrificed at the human endpoint.

(B) Quantification of nuclear TRF1 fluorescence in multiple mouse tissue after *Trf1* deletion in *Ink4Arf*-deficient background (right). Representative images (left). Scale bar, 5 μM.

(C) Quantification of nuclear TRF1 fluorescence in multiple mouse tissue after *Trf1* deletion in *Ink4Arf*-deficient background (right). Representative images (left). Scale bar, 5 μM.

Figure 1. *Continued*

(D) Quantification of nuclear TRF1 fluorescence in multiple mouse tissue after *Trf1* deletion in WT background (right). Representative images (left). Scale bar, 5 μM.

(E–G) (E) qRT-PCR analysis of *Trf1* mRNA expression in *Ink4Arf*-deficient background. (F) qRT-PCR analysis of *Trf1* mRNA expression in *p53*-deficient background. (G) qRT-PCR analysis of *Trf1* mRNA expression in WT background. Data are represented as mean ± SEM. n represents number of mice. Statistical analysis: unpaired *t* test. *p < 0.05, **p < 0.01, ***p < 0.001.

See also Figures S1 and S2.

1E–1G) and PCR analysis (Figures S1E–S1G) in multiple organs from $Trf1^{+/+}$ and $Trf1^{lox/lox}$ mice. Thus, long-term tamoxifen treatment can efficiently delete *Trf1* in different adult mouse tissues.

To address whether long-term *Trf1* deletion was affecting telomere length, we performed quantitative telomere fluorescence *in situ* hybridization (FISH) analysis in intestinal sections from $Trf1^{+/+}$ and $Trf1^{lox/lox}$ mice. We observed that *Trf1* deletion only caused a significant decrease in intestinal telomere length in $Ink4Arf^{-/-}$ mice (Figure S2A).

Interestingly, we found that *Trf1* deletion did not significantly affect overall mouse survival in any of the genetic backgrounds studied (*Ink4Arf*-deficient, *p53*-deficient, and WT backgrounds) (Figure 2A). *Trf1*-deficient mice, however, showed skin abnormalities of different severities depending on the genetic background. In particular, in the *Ink4Arf*-deficient background, *Trf1* deletion caused severe hair graying, whereas this was not observed in the $p53^{-/-}$ background (Figure 2B). In the $p53^{-/-}$ background, *Trf1* deletion caused hair loss and skin wounds (Figure 2B). In the WT background, *Trf1* deletion caused the most severe skin phenotype, including both hair graying and hair loss (Figure 2B), suggesting that loss of the tumor suppressors was partially rescuing the phenotypes induced by *Trf1* deletion.

Longitudinal analysis of body weight also revealed that *Trf1* abrogation in the *Ink4Arf*-deficient background caused a slight but significant decrease in body weight at older ages (6 months of age) only in females (Figures 2C and 2D). Interestingly, this phenotype was not observed in *p53*-deficient male or female mice (Figures 2C and 2D), again suggesting a less severe phenotype in the in *p53*-deficient mice than in the *Ink4Arf*-deficient background. Finally, as the case of the skin, the most severe weight phenotype was observed when *Trf1* was deleted in the WT background, where both males and females showed a significant decrease in body weight, which was more severe in females (Figures 2C and 2D). In summary, full-body *Trf1* deletion did not impair mouse viability in any of the studied genetic backgrounds, although we could observe mild phenotypes like decreased body weight and hair graying or hair loss, which were of different severities in the different genetic backgrounds.

Trf1 Genetic Deletion Induces Epithelial Abnormalities

To further characterize the cellular phenotypes induced by *Trf1* deletion, we performed a full histological analysis of the different $Trf1^{lox/lox}$ and $Trf1^{+/+}$ mouse cohorts. In the case of the *Ink4Arf*-deficient background, we did not see any significant pathologies in the intestine, bone marrow, and the liver of *Trf1*-deleted mice compared with control mice (Figure 3A). However, 85% of $Trf1^{lox/lox}$ $Ink4Arf^{-/-}$ mice showed increased epithelial abnormalities compared with control mice (Figure 3A). We classified the skin lesions as "non-tumoral" and "pre-neoplastic lesions." "Non-tumoral" lesions included degenerative lesions, i.e., atrophy in both epidermis and hypodermis, dermal fibrosis, follicular atrophy, and proliferative lesions, i.e., hyperkeratosis. The pre-neoplastic lesions included cell depolarization and nuclear atypia (i.e., anisocariosis, anisocytosis, and giant nuclei). We found that *Trf1* deficiency in the *Ink4Arf*-deficient background caused a significant increase in both the percentage of mice with "non-tumoral" and "pre-neoplastic" lesions as well as in the number of these lesions per mouse (Figures 3B–3E). Although we did not find any overt intestinal pathologies in $Trf1^{lox/lox}$ *Ink4Arf*-deficient mice, they showed a mild shortening of the intestinal microvilli (Figure 3F).

Interestingly, in the *p53*-deficient background, pathologies associated with *Trf1* deletion were detected in a wider range of tissues including the skin, intestine, stomach, esophagus, and testes, although the differences reached statistical significance only in the skin and the intestine (Figure 4A). In the case of the skin, *Trf1* deletion increased both the percentage of mice with "non-tumoral" and the "pre-neoplasic" lesions as well as the number of these lesions per mouse (Figures 4B and 4C). The most prevalent "non-tumoral" lesions included dermatitis, hyperkeratosis, and hyperplasia (Figure 4D). Regarding the pre-neoplastic lesions, *Trf1* deletion increased the presence of dysplasia, cell depolarization, malignant hyperplasia, and

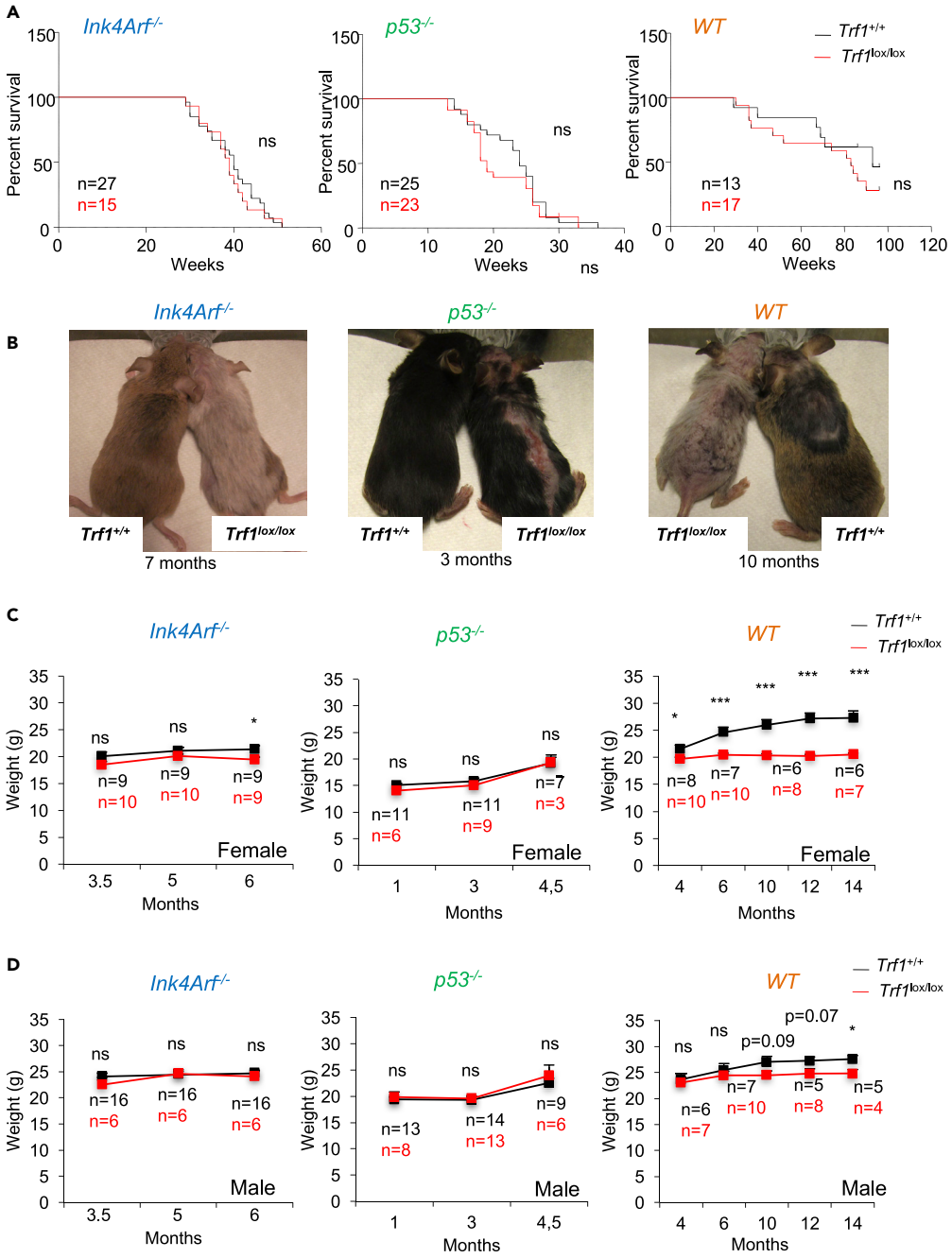

Figure 2. *Trf1* Deletion in *Ink4Arf*-Deficient, *p53*-Deficient, and Wild-Type Backgrounds Does Not Alter Mice Viability

(A) Survival curve analysis of $Trf1^{+/+}$ and $Trf1^{lox/lox}$ mice in *Ink4Arf*-deficient, *p53*-deficient, and wild-type backgrounds.

(B) Representative images of mice of the indicated genotypes.

(C) Weight follow-up in females of the indicated genotypes.

(D) Body weight follow-up in males of the indicated genotypes.

Data are represented as mean ± SEM. n represents number of mice. Statistical analysis: unpaired t test, and log rank test. ns, no significant. *p < 0.05, ***p < 0.001.

nuclear atypia (Figure 4E). Similar results were observed in the intestine, the stomach, and the esophagus. In particular, *Trf1* deletion significantly increased the number of pre-neoplastic lesions in the intestine (Figure 4F), including dysplasia, cell depolarization, and nuclear atypia (Figure 4G). The same tendency

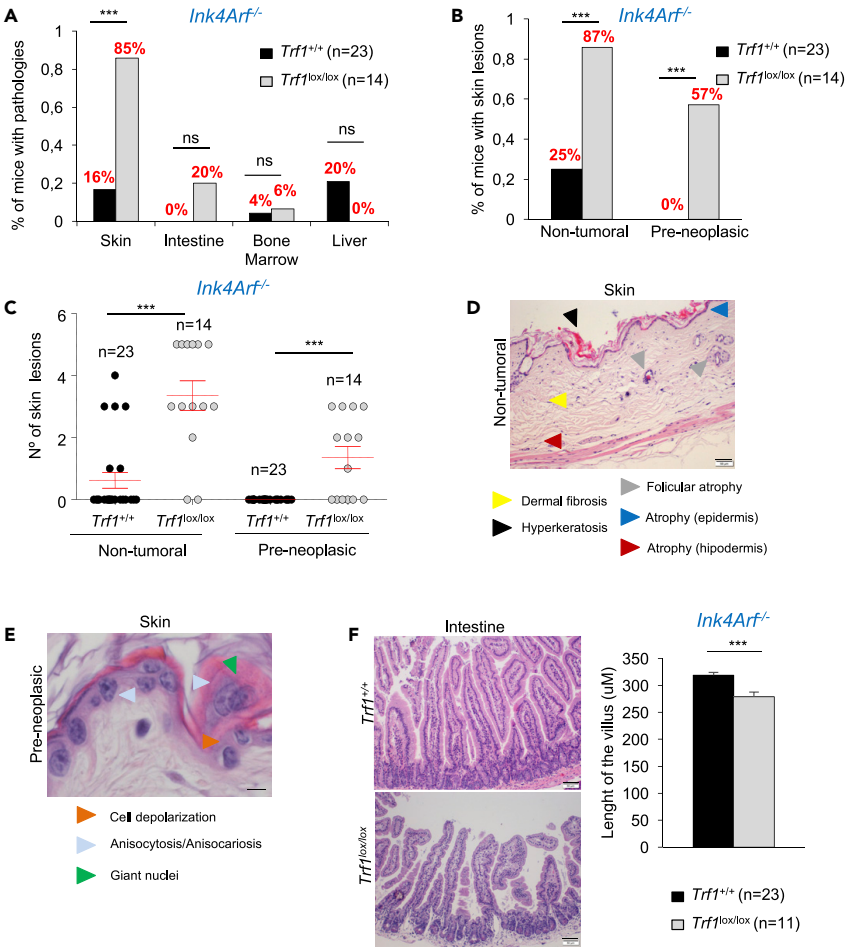

Figure 3. Histopathological Analysis in *Trf1*-Deficient *Ink4Arf*$^{-/-}$ Mice

(A) Percentage of mice with pathologies in skin, intestine, bone marrow, and liver after *Trf1* deletion.

(B) Percentage of *Trf1*$^{+/+}$ and *Trf1*$^{lox/lox}$ mice with "non-tumoral" and "pre-neoplasic" skin lesions.

(C) Number of "non-tumoral" and "pre-neoplasic" skin lesions per mice in the indicated genotypes.

(D) Representative image of skin "non-tumoral" lesions. Scale bar, 50 μM.

(E) Representative image of skin "pre-neoplasic" lesions. Scale bar, 10 μM.

(F) Quantification of the length of the villi in *Trf1*$^{+/+}$ and *Trf1*$^{lox/lox}$ mice (right) and representative images (left). Scale bar, 50 μM. Data are represented as mean ± SEM. n represents number of mice. Statistical analysis: unpaired t test and chi-square test. ns, no significant. ***p < 0.001.

was observed in stomach and esophagus (Figures 4H and 4I), although it did not reach statistical significance. Regarding the reproductive organs, we found that 18% of *Trf1*$^{lox/lox}$ mice suffered from azoospermia in the testes or follicular atrophy in the ovaries (Figure 4A).

Finally, we also determined the effects of *Trf1* deletion in a WT background. In this case, we observed a significant increase in pathologies in the skin and intestine, although it only reached statistical significance in the skin (Figure 5A). In fact, 100% of the *Trf1*-deficient mice showed an increase in skin pathologies (Figure 5A). Interestingly, and contrary to the results obtained in cancer-prone models, all the pathologies found were "non-tumoral" (Figures 5B and 5C), including degenerative lesions like atrophy in both epidermis and hypodermis, dermal fibrosis and follicular atrophy, inflammatory lesions such as dermatitis, and proliferative lesion like benign hyperplasias and hyperkeratosis (Figure 5D).

In summary, *Trf1* deletion increased the presence of non-tumoral lesions in the skin of *Ink4Arf*-deficient, *p53*-deficient, and WT mice. However, the increase in "pre-neoplasic" lesions was only observed in the

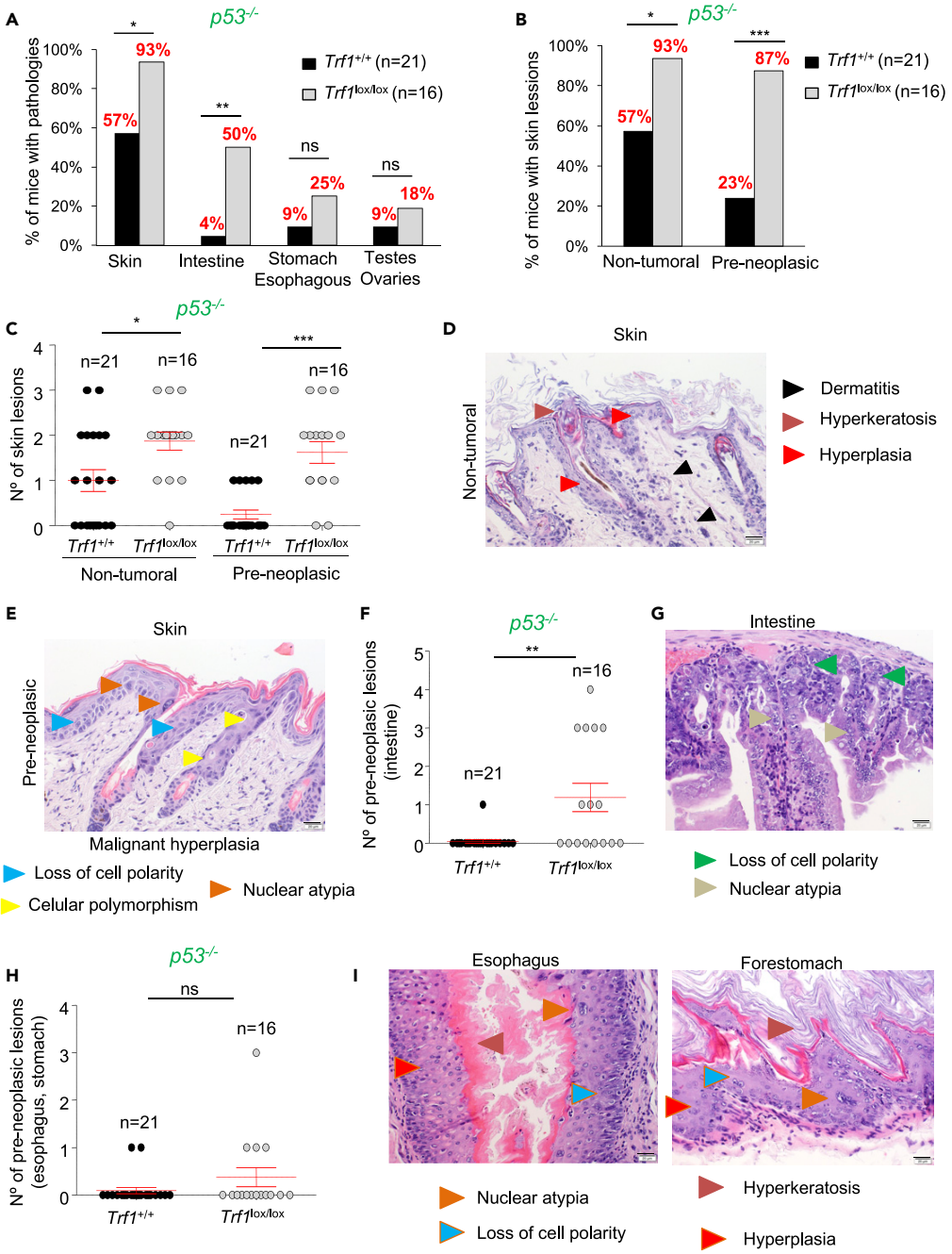

Figure 4. Histopathological Analysis in *Trf1*-Deficient *p53*$^{-/-}$ Mice

(A) Percentage of mice with pathologies in skin, intestine, esophagus, stomach, and testes after *Trf1* deletion.

(B) Percentage of *Trf1*$^{+/+}$ and *Trf1*$^{lox/lox}$ mice with "non-tumoral" and "pre-neoplasic" skin lesions.

(C) Number of "non-tumoral" and "pre-neoplasic" skin lesions per mice of the indicated genotypes.

(D) Representative image of skin "non-tumoral" lesions. Scale bar, 20 μM.

(E) Representative image of skin "pre-neoplasic" lesions. Scale bar, 20 μM.

(F) Number of intestinal "pre-neoplasic" lesions *Trf1*$^{+/+}$ and *Trf1*$^{lox/lox}$ mice.

(G) Representative image of intestinal "pre-neoplasic" lesions.

(H) Number of "pre-neoplasic" lesions in the esophagus and stomach of *Trf1*$^{+/+}$ and *Trf1*$^{lox/lox}$ mice.

(I) Representative image of "pre-neoplasic" lesions in stomach and esophagus. Scale bar, 20 μM.

Data are represented as mean ± SEM. n represents number of mice. Statistical analysis: unpaired t test and chi-square test. ns, no significant. *p < 0.05, **p < 0.01, ***p < 0.001.

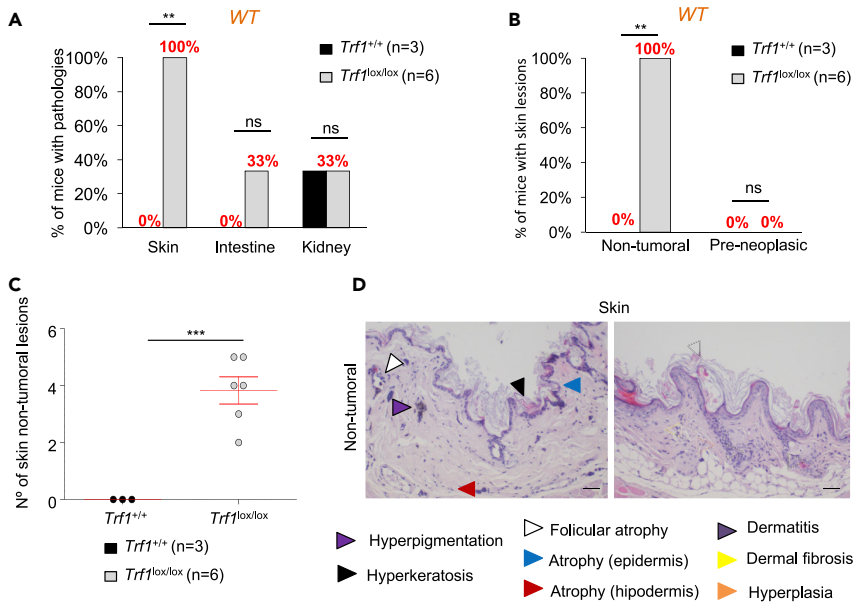

Figure 5. Histopathological Analysis of *Trf1*-Deficient Mice in a Wild-Type Background

(A) Percentage of mice with pathologies in skin, intestine, and kidney after *Trf1* deletion.

(B) Percentage of $Trf1^{+/+}$ and $Trf1^{lox/lox}$ mice with "non-tumoral" and "pre-neoplasic" skin lesions.

(C) Number of "non-tumoral" and "pre-neoplasic" skin lesions per mice of the indicated genotypes.

(D) Representative image of skin "non-tumoral" lesions. Scale bar, 50 μM. Data are represented as mean ± SEM. n represents number of mice. Statistical analysis: unpaired t test and chi-square test. ns, no significant. $^{**}p < 0.01$, $^{***}p < 0.001$.

absence of the tumor suppressors *Ink4Arf* and *p53*, but not when *Trf1* was deleted in a WT background, suggesting that these tumor suppressors mediate some cellular effects of *Trf1* deletion.

Trf1 Deletion Induces DNA Damage and Proliferation Defects, but Does Not Reduce Stem Cell Markers

Trf1 deletion has been previously shown to induce a persistent DDR at telomeres, which can lead to senescence or apoptosis depending on the cell type (Martínez et al., 2009; Beier et al., 2012; Schneider et al., 2013; Povedano et al., 2015). Here, we set to address whether whole-body *Trf1* deletion caused increased DNA damage in the context of WT and tumor-prone models studied here. Given that the most affected tissue was the skin, we quantified the percentage of cells positive for the γH2AX DNA damage marker in skin sections from $Trf1^{lox/lox}$ and $Trf1^{+/+}$ mice in *Ink4Arf*-deficient, *p53*-deficient, and WT backgrounds by using immunohistochemistry (Methods). We found that in a *Ink4Arf*-deficient background, $Trf1^{lox/lox}$ mice showed 12% γH2AX-positive skin cells compared with only 5% in the case of $Trf1^{+/+}$ mice (Figure 6A). Interestingly, in a *p53*-deficient background, $Trf1^{lox/lox}$ mice showed up to 53% of the skin cells positive for γH2AX compared with 6% in the $Trf1^{+/+}$ controls (Figure 6A). In the case of a WT background, *Trf1*-deleted mice showed 18% of the skin cells positive for γH2AX positive compared with 3% in the $Trf1^{+/+}$ controls (Figure 6A). To study whether the DNA damage was stemming from telomeres, we determined the so-called telomere-induced foci (TIF), by performing immuno-FISH analysis with 53BP1 as a marker of DNA damage and the telomeric FISH probe to locate telomeres in skin sections. Again, *Trf1* deletion only increased the percentage of cells with more than one TIF in the *p53*-deficient background (Figure 6B). Together, these findings suggest that *p53* deficiency is allowing for the accumulation of DNA-damaged cells in the skin of $Trf1^{lox/lox}$ mice, whereas these cells are less frequent in the skin of *Ink4Arf*-deficient and WT backgrounds, in agreement with the known role of p53 in signaling telomere-induced DNA damage (Chin et al., 1999; Martínez et al., 2009).

Next, we set to address whether *Trf1* deletion also resulted in cell proliferation defects in the skin. To this end, we quantified the percentage of cells positive for the Ki67 proliferation marker by using immunohistochemistry in skin sections from the different mouse cohorts. In the *Ink4Arf*-deficient background, we

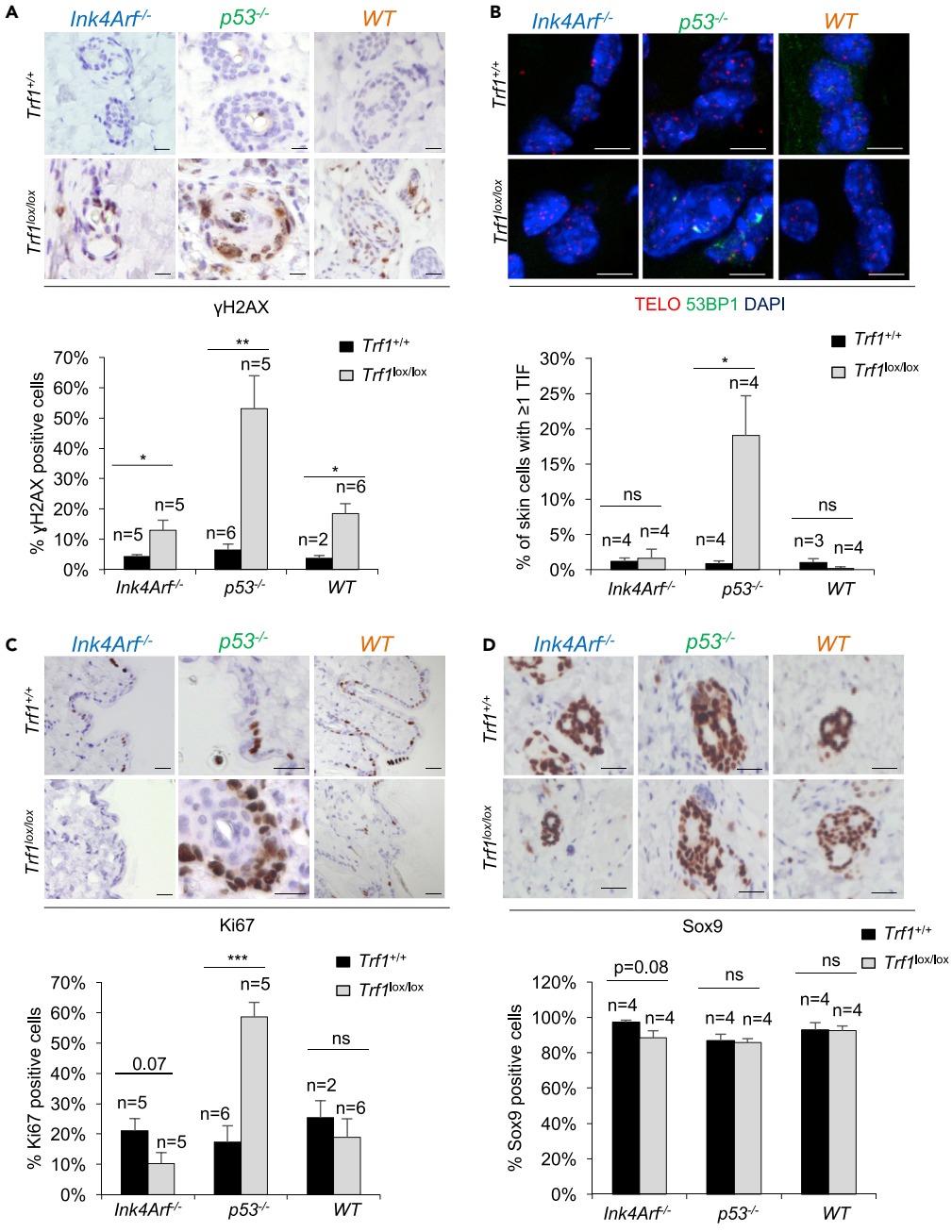

Figure 6. *Trf1* Deletion Leads to DNA Damage And Proliferation Defects in *Ink4Arf*- and *p53*-Deficient Backgrounds

(A) Representative images (up) and quantification (down) of γH2AX -positive cells in the hair follicles after *Trf1* deletion in *Ink4Arf*$^{-/-}$, *p53*$^{-/-}$, and wild-type backgrounds. Scale bar, 10 μM.

(B) Representative images (up) and quantification (down) of percentage of cells with more than 1 TIF after *Trf1* deletion in the indicated genotypes. Scale bar, 5 μM.

(C) Representative images (up) and quantification (down) of Ki67-positive cells in the basal layer after *Trf1* deletion in the indicated genotypes. Scale bar, 20 μM.

(D) Representative images (up) and quantification (down) of Sox9 -positive cells in the hair follicles after *Trf1* deletion in the indicated backgrounds. Scale bar, 20 μM.

Data are represented as mean ± SEM. n represents number of mice. Statistical analysis: unpaired t test. See also Figure S3. ns, no significant. *p < 0.05, **p < 0.01, ***p < 0.001.

found a severe decrease in proliferation with only 10% of the basal layer cells positive for Ki67 compared with more than 20% in the control mice (Figure 6C). In contrast, in the absence of *p53*, *Trf1*$^{lox/lox}$ mice showed a marked increase in proliferation reaching 60% of the basal layer cells being positive for Ki67 compared with 20% in the control counterparts (Figure 6C). In the WT background, however, we did not see significant differences in proliferation between the *Trf1*-deleted and control counterparts (Figure 6C). Again, these results suggest that the *p53* tumor suppressor represents a stronger barrier than the *Ink4Arf* tumor suppressor to prevent the proliferation of cells deficient for *Trf1* and with increased DNA damage, which in turn may favor the increased pre-neoplastic lesions in these backgrounds.

Finally, we determined whether *Trf1* deletion was affecting known skin stem cell makers. To this end, we quantified the percentage of cells positive for the Sox9 skin stem cell marker by using immunohistochemistry in skin sections from *Trf1*$^{+/+}$ and *Trf1*$^{lox/lox}$ mice. However, we did not observe significant differences in Sox9-positive cells in *Trf1*-deleted mice from any of the different genetic backgrounds (Figure 6D). As an independent tissue, we determined the percentage of Sox2-positive cells (a marker of neural stem cells) by immunohistochemistry in the brain, and again we did not observe any differences in the number of Sox2-positive cells between *Trf1*$^{+/+}$ and *Trf1*$^{lox/lox}$ mice in the different genetic backgrounds (Figure S3A).

Tumors Appearing in *Trf1*-Deleted Mice Are Escapers and Express the TRF1 Protein

The absence of both the *Ink4Arf* and the *p53* tumor suppressors has been widely linked to the appearance of spontaneous tumors in mice, including histiocytic sarcomas (HS), sarcomas, or lymphomas (Jacks et al., 1994; Serrano et al., 1996). On the other hand, we have recently demonstrated that *Trf1* deletion has an anti-tumorigenic effect in the context of oncogene-driven tumors in mice by using both lung cancer and glioblastoma mouse models (García-Beccaria et al., 2015; Bejarano et al., 2017). However, even though *Trf1* deletion has an anti-tumorigenic effect in oncogene-induced tumor models, it is also conceivable that DNA damage induced by *Trf1* deletion could promote tumorigenesis in the context of tumor suppressor-deficient mouse models. To explore this possibility, we studied spontaneous tumorigenesis in *Trf1*$^{lox/lox}$ and *Trf1*$^{+/+}$ mice, in both *Ink4Arf*- and *p53*-deficient backgrounds. To this end, we followed mice throughout their entire lifespan and studied the onset and severity of the tumors that appeared.

In a *Ink4Arf* background, *Trf1* deletion did not alter the percentage of mice with tumors (Figure 7A) or the tumor onset (Figure 7B). Interestingly, when looking at particular tumor types, we observed that *Trf1*-deleted mice showed a higher incidence of lymphomas (up to 66%) and a lower incidence of HS and sarcomas, although the two latter ones did not reach statistical significance (Figures 7C and S4A). Although these findings may suggest increased tumorigenesis in the absence of *Ink4Arf*, analysis of TRF1 protein levels in tumors by immunofluorescence revealed that all the lymphomas and HS analyzed in *Trf1*-deficient mice showed normal TRF1 protein levels, indicating that they did not originate from *Trf1*-deleted cells (Figure 7D). The fact that we did not find a single tumor lacking TRF1 expression indicates that TRF1 deficiency impedes tumorigenesis in *Ink4Arf*-deficient background.

In the case of the *p53*-deficient background, *Trf1*-deleted mice reduced the percentage of mice with tumors from 90% (*Trf1*$^{+/+}$) to 68% (*Trf1*$^{lox/lox}$) (Figure 7E), although this difference did not reach statistical significance. Similarly, we did not observe any differences in tumor onset between *Trf1*$^{+/+}$ and *Trf1*$^{lox/lox}$ mice (Figure 7F). When looking at individual tumor types, we observed a tendency to show decreased thymic lymphomas and sarcomas in the *Trf1*$^{lox/lox}$ mice (Figures 7G and S4B), although the difference did not reach statistical significance. In contrast, we observed a significant increase in skin carcinomas in *Trf1*$^{lox/lox}$ mice (Figures 7G and S4B). However, TRF1 immunofluorescence analysis indicated that all the tumors appearing in *Trf1*$^{lox/lox}$ mice were escapers, as no differences were found in TRF1 protein levels compared with the *Trf1*$^{+/+}$ mice (Figure 7H). Note that for skin carcinomas we used normal skin of *Trf1*$^{+/+}$ mice as control as these types of tumors were not found in control mice.

These findings indicate that *Trf1* deficiency completely blocks tumorigenesis in the context of mice deficient for two major tumor suppressors, *Ink4Arf* and *p53*.

DISCUSSION

Therapeutic strategies based on telomerase inhibition have been the focus of cancer treatments for some years, as telomere maintenance above a minimum length is necessary for cancer cell growth (Kim et al., 1994; Hanahan and Weinberg, 2011). However, both telomerase abrogation in mouse models and human

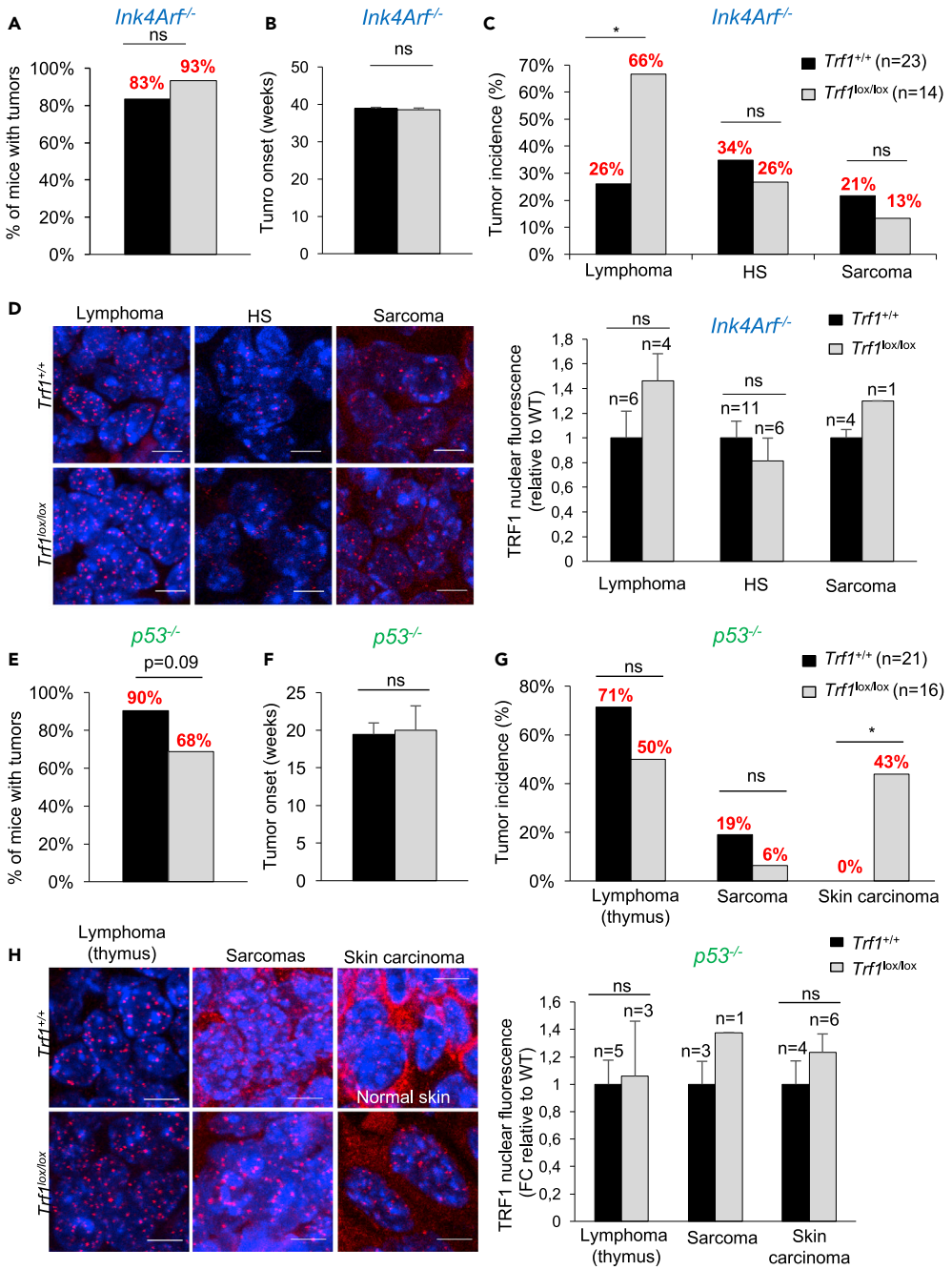

Figure 7. *Trf1* Deletion Blocks Tumorigenesis in *InkArf*-Deficient and *p53*-Deficient Mice

(A) Percentage of mice with tumors at the human endpoint in $Trf1^{+/+}$ and $Trf1^{lox/lox}$ *InkArf*-deficient mice.

(B) Tumor onset in the indicated genotypes.

(C) Lymphoma, HS, and sarcoma incidences in $Trf1^{+/+}$ and $Trf1^{lox/lox}$ *InkArf*-deficient mice.

(D) Quantification (right) and representative images (left) of nuclear TRF1 fluorescence in $Trf1^{+/+}$ and $Trf1^{lox/lox}$ mouse tumors. Scale bar, 5 μM.

(E) Percentage of mice with tumors at the human endpoint in $Trf1^{+/+}$ and $Trf1^{lox/lox}$ *p53*-deficient mice.

(F) Tumor onset in the indicated genotypes.

(G) Thymoma, sarcoma, and skin carcinoma incidence in $Trf1^{+/+}$ and $Trf1^{lox/lox}$ *p53*-deficient mice.

(H) Quantification (right) and representative images (left) of nuclear TRF1 fluorescence in $Trf1^{+/+}$ and $Trf1^{lox/lox}$ mouse tumors. Note that normal skin of $Trf1^{+/+}$ mice was used as control for skin carcinomas. Scale bar, 5 μM.

Data are represented as mean ± SEM. n represents number of mice. Statistical analysis: unpaired t test and chi-square test. See also Figure S4. ns, no significant. *$p < 0.05$.

clinical trials with telomerase inhibitors have shown limitations, most likely owing to the fact that a telomerase inhibitor would be only effective when telomeres are short and tumors are heterogeneous in terms of telomere length as well as can activate telomerase-independent mechanisms for telomere length maintenance or ALT (Chin et al., 1999; Greenberg et al., 1999; Gonzalez-Suarez et al., 2000; Parkhurst et al., 2004; Perera et al., 2008; Middleton et al., 2014).

We have recently proposed an alternative strategy for targeting the telomeres independently of telomere length by directly targeting the telomere-protective complex shelterin through TRF1 inhibition. TRF1 is an essential component of shelterin that directly binds TTAGGG telomeric DNA repeats (De Lange, 2005; Martínez and Blasco, 2011). *Trf1* genetic deletion *in vivo* induces a persistent DDR at telomeres, which is sufficient to block cell division and induce apoptosis or senescence in several mouse tissues (Martínez et al., 2009; Beier et al., 2012; Schneider et al., 2013; Povedano et al., 2015). Interestingly, induction of telomere uncapping by *Trf1* genetic depletion or TRF1 chemical inhibition can effectively block the growth of very aggressive and rapidly growing lung tumors in *p53*-deficient *K-RasG12V* mice, in a manner that is independent of telomere length (García-Beccaria et al., 2015), as well as can block both tumor initiation and progression in glioblastoma mouse models (Bejarano et al., 2017).

Any potential anti-cancer target must fulfill the important requisite of not showing deleterious effects in healthy tissues or compromising organism viability. In line with this, we had previously demonstrated that short-term *Trf1* full-body deletion does not impair organism viability or cognitive functions and only affects slightly the highly proliferative tissues (García-Beccaria et al., 2015; Bejarano et al., 2017). However, the long-term effects of *Trf1* deletion are still unknown.

Here we set to address the long-term effects of *Trf1* whole-body deletion in three different genetic backgrounds, including WT mice and the cancer-prone *Ink4Arf*$^{-/-}$ and *p53*$^{-/-}$ mouse models. We show that full-body *Trf1* deletion does not impair mouse viability in any of the studied genetic backgrounds, although we could observe mild phenotypes like decreased body weight and hair graying or hair loss, which were more severe in the WT background. In all the studied genetic backgrounds the most affected tissue was the skin. In fact, *Trf1* deletion increased the presence of "non-tumoral," mainly degenerative, lesions in the skin in all the studied backgrounds. Interestingly, we also observed an increase in pre-neoplastic lesions, but only in the absence of the tumor suppressors *Ink4Arf* and *p53*. At the cellular level, we observed that *Trf1* deletion induced different degrees of DNA damage in the skin of all genetic backgrounds although we only observed increased proliferation in the case of the *p53*-deficient background, in line with the known role of *p53* in signaling proliferation arrest in the presence of dysfunctional telomeres. Importantly, we did not observe significantly decreased stem cell markers in the skin or the brain upon conditional *Trf1* deletion, suggesting that tissue homeostasis is largely preserved upon *Trf1* deletion, in agreement with normal survival of *Trf1*-deleted mice in all genetic backgrounds.

We previously showed that *Trf1* deletion can block the growth of oncogene-driven, aggressive lung and glioblastoma tumors by inducing DNA damage at chromosome ends (García-Beccaria et al., 2015; Bejarano et al., 2017). However, it was still unclear whether persistent *Trf1* deletion in the absence of an oncogenic driver could eventually lead to a high genomic instability and promote tumorigenesis. To explore this idea, we studied spontaneous tumorigenesis in *Trf1*$^{lox/lox}$ and *Trf1*$^{+/+}$ mice, in both *Ink4Arf*- and *p53*-deficient backgrounds. The absence of both the *Ink4Arf* and the *p53* tumor suppressors has been widely linked to the appearance of spontaneous tumors in mice, including HS, sarcomas, or lymphomas (Jacks et al., 1994; Serrano et al., 1996). The results described here clearly indicate that *Trf1* deletion does not increase the percentage of mice with tumors in the absence of the tumor suppressors, although for certain tumor types, like lymphomas in the *Ink4Arf*-deficient background and skin carcinomas in the case of the *p53*-deleted mice, we found an increased incidence upon *Trf1* deletion. However, analysis of TRF1 protein levels in these tumors revealed that they were not deficient for TRF1 as they showed normal TRF1 protein levels, indicating that they did not originate from *Trf1*-deleted cells. The fact that no tumors lacking TRF1 expression were found suggests that TRF1 is essential for tumorigenesis in both *Ink4Arf*-deficient and *p53*-deficient backgrounds.

In light of these findings, one could argue that TRF1 inhibition in cancer could be advantageous compared with classical chemotherapies that are known to induce severe DNA damage, as well as induction of

premature aging effects and of secondary tumors. In summary, these findings support that there is a therapeutic window for targeting TRF1 in cancer treatment.

Limitations of the Study

The limitation of this study is that Cre-mediated *Trf1* deletion is not 100% in every organ, as reported by the immunofluorescence data. Thus, it should be considered that the observed phenotype is the consequence of a 50%–70% *Trf1* deletion.

METHODS

All methods can be found in the accompanying Transparent Methods supplemental file.

SUPPLEMENTAL INFORMATION

Supplemental Information can be found online at https://doi.org/10.1016/j.isci.2019.08.012.

ACKNOWLEDGMENTS

We thank R. Serrano for mice handling and the Comparative Pathology and Mouse Facility Units at CNIO. M.A.B. laboratory is funded by SAF2013-45111-R from MINECO, *Fundación Botín*, and Banco Santander and Worldwide Cancer Research 16-1177. L.B. is a fellow of the La Caixa-Severo Ochoa International PhD Program.

AUTHOR CONTRIBUTIONS

M.A.B. and L.B. designed the experiments and wrote the manuscript; L.B., J.L., and J.J.M. performed the experiments; D.M. performed the IF quantifications; J.M.F. performed the histopathological analysis.

DECLARATION OF INTERESTS

The authors declare that they have no conflict of interest.

Received: May 28, 2019
Revised: July 28, 2019
Accepted: August 5, 2019
Published: September 27, 2019

REFERENCES

Bainbridge, M.N., Armstrong, G.N., Gramatges, M.M., Bertuch, A.A., Jhangiani, S.N., Doddapaneni, H., Lewis, L., Tombrello, J., Tsavachidis, S., Liu, Y., Jalali, A., et al. (2015). Germline mutations in shelterin complex genes are associated with familial glioma. J. Natl. Cancer Inst. *107*, 384.

Barthel, F.P., Wei, W., Tang, M., Martinez-Ledesma, E., Hu, X., Amin, S.B., Akdemir, K.C., Seth, S., Song, X., Wang, Q., Lichtenberg, T., Hu, J., et al. (2017). Systematic analysis of telomere length and somatic alterations in 31 cancer types. Nat. Genet. https://doi.org/10.1038/ng.3781.

Beier, F., Foronda, M., Martinez, P., and Blasco, M.A. (2012). Conditional TRF1 knockout in the hematopoietic compartment leads to bone marrow failure and recapitulates clinical features of dyskeratosis congenita. Blood *120*, 2990–3000.

Bejarano, L., Schuhmacher, A.J., Méndez, M., Megías, D., Blanco-Aparicio, C., Martínez, S., Pastor, J., Squatrito, M., and Blasco, M.A. (2017). Inhibition of TRF1 telomere protein impairs tumor initiation and progression in glioblastoma mouse models and patient-derived xenografts. Cancer Cell *32*, 590–607.e4.

Boué, S., Paramonov, I., Barrero, M.J., and Belmonte, J.C.I. (2010). Analysis of human and mouse reprogramming of somatic cells to induced pluripotent stem cells. What is in the plate? PLoS One *5*, 1–14.

Bryan, T.M., Englezou, A., Dalla-Pozza, L., Dunham, M.A., and Reddel, R.R. (1997). Evidence for an alternative mechanism for maintaining telomere length in human tumors and tumor-derived cell lines. Nat. Med. *3*, 1271–1274.

Calvete, O., Martinez, P., Garcia-Pavia, P., Benitez-Buelga, C., Paumard-Hernández, B., Fernandez, V., Dominguez, F., Salas, C., Romero-Laorden, N., Garcia-Donas, J., Carrillo, J., et al. (2015). A mutation in the POT1 gene is responsible for cardiac angiosarcoma in TP53-negative Li-Fraumeni-like families. Nat. Commun. *6*, 8383.

Chin, L., Artandi, S.E., Shen, Q., Tam, A., Lee, S.L., Gottlieb, G.J., Greider, C.W., and DePinho, R.A. (1999). p53 deficiency rescues the adverse effects of telomere loss and cooperates with telomere dysfunction to accelerate carcinogenesis. Cell *97*, 527–538.

García-Beccaria, M., Martínez, P., Méndez-Pertuz, M., Martínez, S., Blanco-Aparicio, C., Cañamero, M., Mulero, F., Ambrogio, C., Flores, J.M., Megias, D., Barbacid, M., et al. (2015). Therapeutic inhibition of TRF1 impairs the growth of p53-deficient K-RasG12V-induced lung cancer by induction of telomeric DNA damage. EMBO Mol. Med. *7*, 930–949.

Gonzalez-Suarez, E., Samper, E., Flores, J.M., and Blasco, M.A. (2000). Telomerase-deficient mice with short telomeres are resistant to skin tumorigenesis. Nat. Genet. *26*, 114–117.

Greenberg, R.A., Chin, L., Femino, A., Kee-Ho, L., Gottlieb, G.J., Singer, R.H., Greider, C.W., and DePinho, R.A. (1999). Short dysfunctional telomeres impair tumorigenesis in the INK4a(??2/3) cancer-prone mouse. Cell *97*, 515–525.

Greider, C.W., and Blackburn, E.H. (1985). Identification of a specific telomere terminal transferase activity in tetrahymena extracts. Cell *43* (2 PART 1), 405–413.

Hanahan, D., and Weinberg, R.A. (2011). Hallmarks of cancer: the next generation. Cell, 646–674.

Harley, C.B. (2008). Telomerase and cancer therapeutics. Nat. Rev. Cancer, 167–179.

Harley, C.B., Futcher, A.B., and Greider, C.W. (1990). Telomeres shorten during ageing of human fibroblasts. Nature *345*, 458–460.

Hu, H., Zhang, Y., Zou, M., Yang, S., and Liang, X.Q. (2010). Expression of TRF1, TRF2, TIN2, TERT, KU70, and BRCA1 proteins is associated with telomere shortening and may contribute to multistage carcinogenesis of gastric cancer. J. Cancer Res. Clin. Oncol. *136*, 1407–1414.

Jacks, T., Remington, L., Williams, B.O., Schmitt, E.M., Halachmi, S., Bronson, R.T., and Weinberg, R.A. (1994). Tumor spectrum analysis in p53-mutant mice. Curr. Biol. *4*, 1–7.

Joseph, I., Tressler, R., Bassett, E., Harley, C., Buseman, C.M., Pattamatta, P., Wright, W.E., Shay, J.W., and Go, N.F. (2010). The telomerase inhibitor imetelstat depletes cancer stem cells in breast and pancreatic cancer cell lines. Cancer Res. *70*, 9494–9504.

Kim, N., Piatyszek, M., Prowse, K., Harley, C., West, M., Ho, P., Coviello, G., Wright, W., Weinrich, S., and Shay, J. (1994). Specific association of human telomerase activity with immortal cells and cancer. Science *266*, 2011–2015.

De Lange, T. (2005). Shelterin: the protein complex that shapes and safeguards human telomeres. Genes Dev. *19*, 2100–2110.

Liu, D., O'Connor, M.S., Qin, J., and Songyang, Z. (2004). Telosome, a mammalian telomere-associated complex formed by multiple telomeric proteins. J. Biol. Chem. *279*, 51338–51342.

Martinez, P., Thanasoula, M., Carlos, A.R., Gómez-López, G., Tejera, A.M., Schoeftner, S., Dominguez, O., Pisano, D.G., Tarsounas, M., and Blasco, M.A. (2010). Mammalian Rap1 controls telomere function and gene expression through binding to telomeric and extratelomeric sites. Nat. Cell Biol. *12*, 768–780.

Martínez, P., Thanasoula, M., Muñoz, P., Liao, C., Tejera, A., McNees, C., Flores, J.M., Fernández-Capetillo, O., Tarsounas, M., and Blasco, M.A. (2009). Increased telomere fragility and fusions resulting from TRF1 deficiency lead to degenerative pathologies and increased cancer in mice. Genes Dev. *23*, 2060–2075.

Martínez, P., and Blasco, M.A. (2011). Telomeric and extra-telomeric roles for telomerase and the telomere-binding proteins. Nat. Rev. Cancer *11*, 161–176.

Middleton, G., Silcocks, P., Cox, T., Valle, J., Wadsley, J., Propper, D., Coxon, F., Ross, P., Madhusudan, S., Roques, T., Cunningham, D., et al. (2014). Gemcitabine and capecitabine with or without telomerase peptide vaccine GV1001 in patients with locally advanced or metastatic pancreatic cancer (TeloVac): an open-label, randomised, phase 3 trial. Lancet Oncol. *15*, 829–840.

Newey, P.J., Nesbit, M.A., Rimmer, A.J., Attar, M., Head, R.T., Christie, P.T., Gorvin, C.M., Stechman, M., Gregory, L., Mihai, R., Sadler, G., et al. (2012). Whole-exome sequencing studies of nonhereditary (sporadic) parathyroid adenomas. J. Clin. Endocrinol. Metab. *97*, E1995–E2005.

Pal, D., Sharma, U., Singh, S.K., Kakkar, N., and Prasad, R. (2015). Over-expression of telomere binding factors (TRF1 & TRF2) in renal cell carcinoma and their inhibition by using SiRNA induce apoptosis, reduce cell proliferation and migration in vitro. PLoS One *10*, https://doi.org/10.1371/journal.pone.0115651.

Parkhurst, M.R., Riley, J.P., Igarashi, T., Li, Y., Robbins, P.F., and Rosenberg, S.A. (2004). Immunization of patients with the hTERT:540-548 peptide induces peptide-reactive T lymphocytes that do not recognize tumors endogenously expressing telomerase. Clin. Cancer Res. *10*, 4688–4698.

Perera, S.A., Maser, R.S., Xia, H., McNamara, K., Protopopov, A., Chen, L., Hezel, A.F., Kim, C.F., Bronson, R.T., Castrillon, D.H., Chin, L., et al. (2008). Telomere dysfunction promotes genome instability and metastatic potential in a K-ras p53 mouse model of lung cancer. Carcinogenesis *29*, 747–753.

Povedano, J.M., Martinez, P., Flores, J.M., Mulero, F., and Blasco, M.A. (2015). Mice with pulmonary fibrosis driven by telomere dysfunction. Cell Rep. *12*, 286–299.

Ramsay, A.J., Quesada, V., Foronda, M., Conde, L., Martínez-Trillos, A., Villamor, N., Rodríguez, D., Kwarciak, A., Garabaya, C., Gallardo, M., López-Guerra, M., et al. (2013). POT1 mutations cause telomere dysfunction in chronic lymphocytic leukemia. Nat. Genet. *45*, 526–530.

Robles-Espinoza, C.D., Harland, M., Ramsay, A.J., Aoude, L.G., Quesada, V., Ding, Z., Pooley, K.A., Pritchard, A.L., Tiffen, J.C., Petljak, M., Palmer, J.M., et al. (2014). POT1 loss-of-function variants predispose to familial melanoma. Nat. Genet. *46*, 478–481.

Schneider, R.P., Garrobo, I., Foronda, M., Palacios, J.A., Marión, R.M., Flores, I., Ortega, S., and Blasco, M.A. (2013). TRF1 is a stem cell marker and is essential for the generation of induced pluripotent stem cells. Nat. Commun. *4*, 1946.

Serrano, M., Lee, H.W., Chin, L., Cordon-Cardo, C., Beach, D., and DePinho, R.A. (1996). Role of the INK4a locus in tumor suppression and cell mortality. Cell *85*, 27–37.

Shay, J.W., and Bacchetti, S. (1997). A survey of telomerase activity in human cancer. Eur. J. Cancer *33*, 787–791.

Shi, J., Yang, X.R., Ballew, B., Rotunno, M., Calista, D., Fargnoli, M.C., Ghiorzo, P., Bressac-de Paillerets, B., Nagore, E., Avril, M.F., Caporaso, N.E., et al. (2014). Rare missense variants in POT1 predispose to familial cutaneous malignant melanoma. Nat. Genet. *46*, 482–486.

Zhang, J., Jima, D., Moffitt, A.B., Liu, Q., Czader, M., Hsi, E.D., Fedoriw, Y., Dunphy, C.H., Richards, K.L., Gill, J.I., Sun, Z., et al. (2014). The genomic landscape of mantle cell lymphoma is related to the epigenetically determined chromatin state of normal B cells,. Blood *123*, 2988–2996.

ISCI, Volume *19*

Supplemental Information

Safety of Whole-Body Abrogation of the TRF1 Shelterin Protein in Wild-Type and Cancer-Prone Mouse Models

Leire Bejarano, Jessica Louzame, Juán José Montero, Diego Megías, Juana M. Flores, and Maria A. Blasco

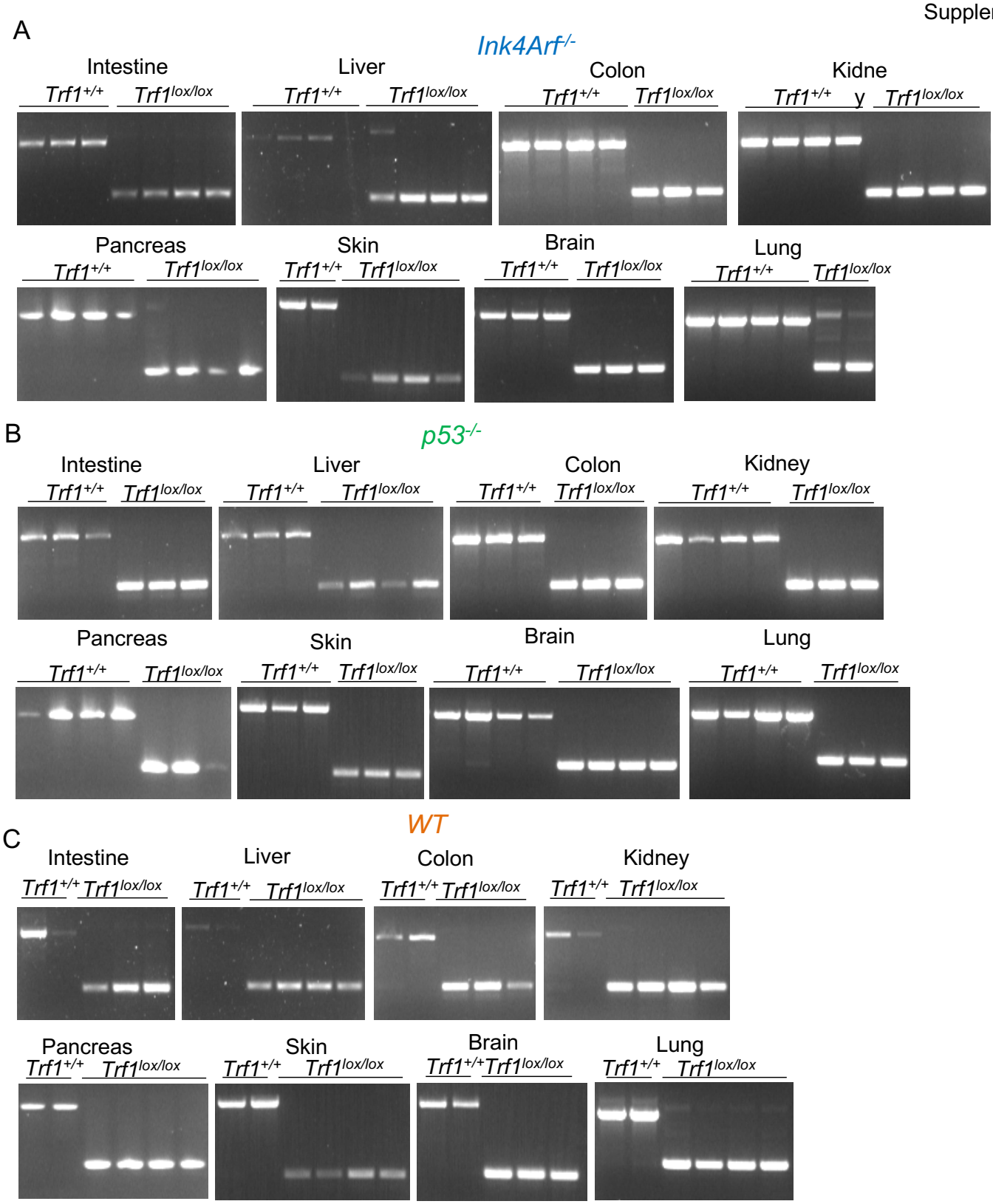
A
Ink4Arf-/-
Intestine
Trf1+/+ Trf1lox/lox
Liver
Trf1+/+ Trf1lox/lox
Colon
Trf1+/+ Trf1lox/lox
Kidne
Trf1+/+ y Trf1lox/lox
Pancreas
Trf1+/+ Trf1lox/lox
Skin
Trf1+/+ Trf1lox/lox
Brain
Trf1+/+ Trf1lox/lox
Lung
Trf1+/+ Trf1lox/lox
B
p53-/-
Intestine
Trf1+/+ Trf1lox/lox
Liver
Trf1+/+ Trf1lox/lox
Colon
Trf1+/+ Trf1lox/lox
Kidney
Trf1+/+ Trf1lox/lox
Pancreas
Trf1+/+ Trf1lox/lox
Skin
Trf1+/+ Trf1lox/lox
Brain
Trf1+/+ Trf1lox/lox
Lung
Trf1+/+ Trf1lox/lox
C
WT
Intestine
Trf1+/+ Trf1lox/lox
Liver
Trf1+/+ Trf1lox/lox
Colon
Trf1+/+ Trf1lox/lox
Kidney
Trf1+/+ Trf1lox/lox
Pancreas
Trf1+/+ Trf1lox/lox
Skin
Trf1+/+ Trf1lox/lox
Brain
Trf1+/+Trf1lox/lox
Lung
Trf1+/+ Trf1lox/lox

A

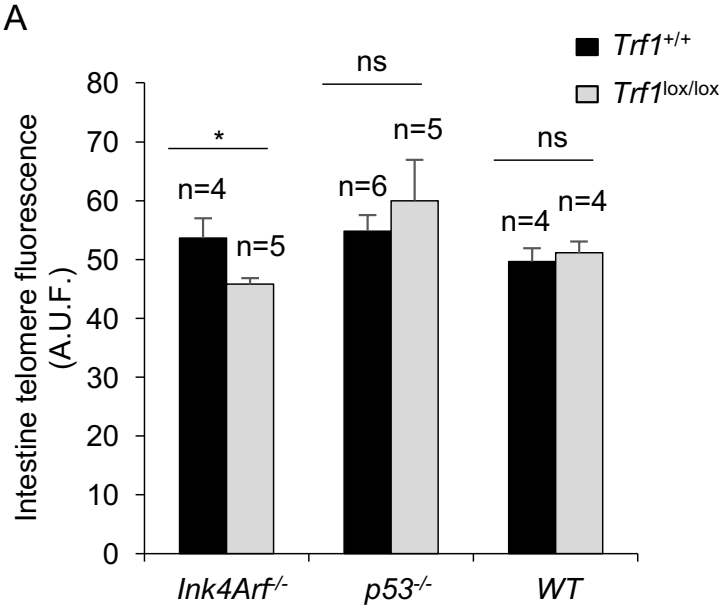
Trf1+/+
Trf1lox/lox
Intestine telomere fluorescence (A.U.F.)
80
70
60
50
40
30
20
10
0
*
ns
ns
n=4
n=5
n=6
n=5
n=4
n=4
Ink4Arf-/-
p53-/-
WT

A

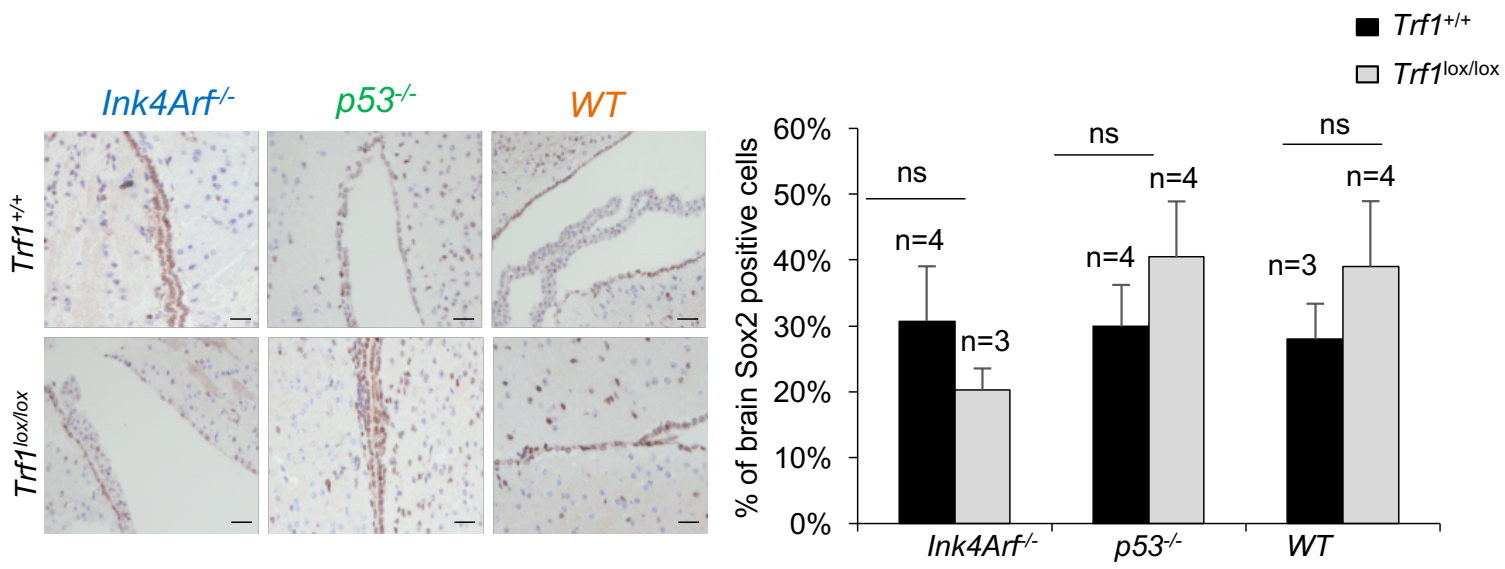
Ink4Arf-/-
p53-/-
WT
Trf1+/+
Trf1lox/lox
Trf1+/+
Trf1lox/lox
% of brain Sox2 positive cells
60%
50%
40%
30%
20%
10%
0%
ns
ns
ns
n=4
n=3
n=4
n=4
n=3
n=4
Ink4Arf-/-
p53-/-
WT

Supplemetary Figure 4

A

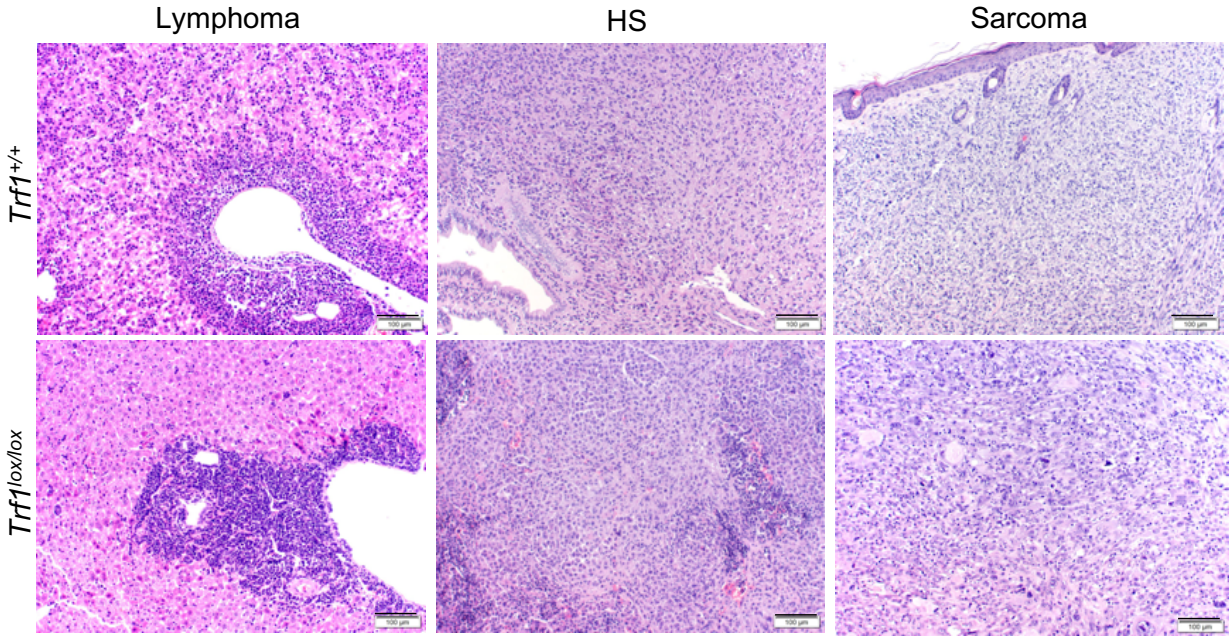

B

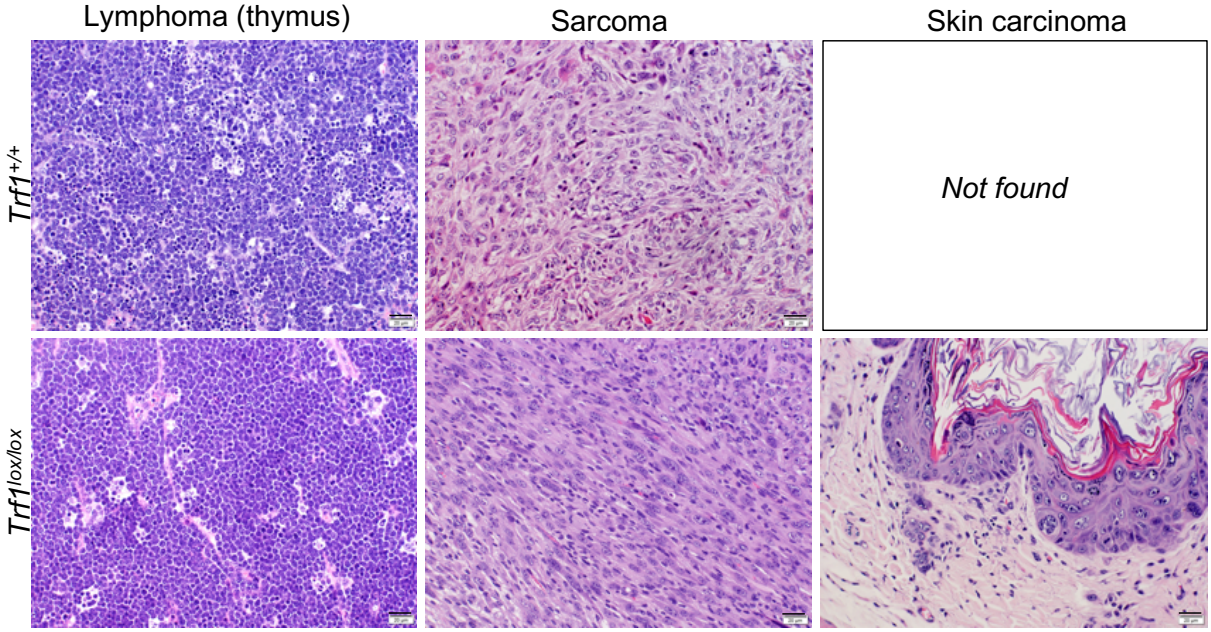

Supplementary figure legends

Supplementary Figure 1. PCR analysis of *Trf1* deletion upon tamoxifen treatment. Related to Figure 1. (A) Analysis of *Trf1* excision by PCR in *Ink4Arf*-deficient mice. (**B**) Analysis of *Trf1* excision by PCR in *p53*-deficient mice. (**C**) Analysis of *Trf1* excision by PCR in wild-type backgorund.

Supplementary Figure 2. Telomere length analysis upon *Trf1* deletion in the different genetic backgrounds. Related to Figure 1. (A) Telomere Q-FISH analysis in the intestine of the indicated genotypes. Data are represented as mean ± SEM. n represents number of mice. Statistical analysis: unpaired *t-test.*

Suplementary Figure 3. *Trf1* deletion does not decrease brain stem cell markers. Related to Figure 6. (A) Representative images (up) and quantification (down) of Sox2 -positive cells in the brain after *Trf1* deletion in the indicated backgrounds. Scale bar 20 μM. Data are represented as mean ± SEM. n represents number of mice. Statistical analysis: unpaired *t-test.*

Supplementary Figure 4. Tumor histology in *InkArf*-deficient and *p53*-deficient mice. Related to Figure 7. (A) Representative images of the different tumor types by H&E at the human end-point. Scale bar 100 μM. **(B)** Representative images of the different tumor types by H&E at the human end-point. Scale bar 20 μM.

Transparent Methods

Mice

Trf1$^{lox/lox}$ mice (Martínez *et al.*, 2009) were crossed with a mouse strain carrying ubiquitously expressed, tamoxifen-activated recombinase, *hUBC-CreERT2* (Ruzankina *et al.*, 2007) to generate *Trf1*$^{lox/lox}$ *or Trf1*$^{+/+}$*, hUBC-CreERT2* mice. These mice were further crossed with *Ink4Arf*$^{-/-}$ (Serrano *et al.*, 1996) and *p53*$^{-/-}$ (Jacks *et al.*, 1994) mouse lines to generate *Trf1*$^{+/+}$ or *Trf1*$^{lox/lox}$*, hUBC-CreERT2, Ink4Arf*$^{-/-}$ and *Trf1*$^{+/+}$ or *Trf1*$^{lox/lox}$*, hUBC-CreERT2, p53*$^{-/-}$ mice. These mice were fed *ad libitum* with tamoxifen containing diet for long-term, starting at 6 weeks of age for *p53*-deficient background and 10-weeks of age for *Ink4Arf*-deficient and wild type backgrounds. *p53*-deficient mice started tamoxifen treatment earlier due to the shorter lifespan of this mice. All mice were maintained at the Spanish National Cancer Centre under specific pathogen-free conditions in accordance with the recommendations of the Federation of European Laboratory Animal Science Associations (FELASA). All animal experiments were approved by the Ethical Committee (CEIyBA) from the Spanish National Cancer Centre and performed in accordance with the guidelines stated in the International Guiding Principles for Biomedical Research Involving Animals, developed by the Council for International Organizations of Medical Sciences (CIOMS).

Immunofluorescence analyses in tissue sections

For immunofluorescence analyses, tissues were fixed in 10% buffered formalin (Sigma) and embedded in paraffin. After despparafination and citrate antigen retrieval,

sections were permeabilized with 0.5% Triton in PBS and blocked with 1%BSA and 10% Australian FBS (GENYCELL) in PBS.

Rat polyclonal anti-TRF1 antibody (homemade) was applied overnight in antibody diluents with background reducing agents (Invitrogen). Anti-rat Alexa 555 secondary antibody (Life Technologies, S.A) was incubated 1 hr at room temperature also in antibody diluents with background reducing agents (Invitrogen).

Immunofluorescence images were obtained using a confocal ultraspectral microscope (Leica TCS-SP5). Quantifications were performed with Definiens software.

Immunohistochemistry analyses in tissue sections

For immunohistochemistry analyses, tissues were fixed in 10% buffered formalin (Sigma) and embedded in paraffin. Immunohistochemistry was performed on de-paraffinated tissue sections processed with 10 mM sodium citrate (pH 6.5) cooked under pressure for 2 min. Slides were washed in water, then in Buffer TBS Tween20 0.5 %, blocked with peroxidase, washed with TBS Tween20 0.5 % again and blocked with fetal bovine serum followed by another wash.

Primary antibodies included those raised against: γH2AX Ser 139 (Millipore), Ki67 (Master diagnostica), Sox2 (C70B1, Cell signaling) and Nestin (RAT-401, Millipore). Slides were then incubated with secondary antibodies conjugated with peroxidase from DAKO.

Pictures were taken using Olympus AX70 microscope. The percentage of positive cells was identified by eye.

Histological analyses in tissue sections

Tissue samples were fixed overnight in 10% neutral buffered formalin, embedded in paraffin and sectioned 3 µm thick and dried. Slides were dewaxed and re-hydrated through a series of graded ethanol until water and were stained with hematoxilin-eosin (H-E). Histological observations and photomicrography were performed using an Olympus DP73 digital camera. Histopathologies were classified into “non-tumoral” lesions, “preneoplasic” lesions and tumor lesions.

“Non-tumoral” lesions included degenerative lesions (atrophy in both epidermis and hypodermis, dermal fibrosis, follicular atrophy), inflammatory lesions (dermatitis, hepatitis) and proliferative lesion (benign hyperplasias, hyperkeratosis).

“Pre-neoplasic” lesions were mainly proliferative and included epithelial dysplasia, malignant hyperplasia, nuclear atypia and cell depolarization.

Tumor lesions were characterized by cellular polymorphism, irregular stratification, both loss of polarity or basement membrane disruption of epithelial cells, nuclear hyperchromatism, nuclear atypia, enlarged nucleoli, increase number of mitotic figures and atypical mitotic figures. The most frequent tumors were lymphomas (in thymus or extending and infiltrating different organs, mainly the spleen, liver, and lymph nodes), histiocytic sarcomas (in liver, spleen and mesenteric lymph nodes), subcutaneous fibrosarcomas and angiosarcomas, vertebral osteosarcomas and squamous cell carcinomas (SCC) in skin.

Telomere length analyses on tissue sections

For quantitative telomere fluorescence *in situ* hybridization (Q-FISH) we deparaffinized paraffin-embedded sections and fixed them with 4% formaldehyde, followed by digestion with pepsine/HCl and a second fixation with 4% formaldehyde. Next, we dehydrated the sides with increasing concentrations of EtOH (70%, 90%,

100% and incubated them with the telomeric probe for 3.5 min at 85ºC followed by 2h RT incubation in a wet chamber. After, the slides were extensively washed with 50% formamide and 0.08% TBS-Tween. Immunofluorescence images were obtained using a confocal ultraspectral microscope (Leica TCS-SP5) and the analysis was performed by Definiens software.

Real-time qPCR

Total RNA from frozen tissue was extracted with the RNeasy kit (QIAGEN) following manufacturer´s instructions. The cDNA synthesis was performed using the iSCRIPT cDNA synthesis kit (BIO-RAD) according to manufacturer's protocols.

Quantitative real-time PCR was performed with the QuantStudio 6 Flex (Applied Biosystems, Life Technologies) using Go-Taq qPCR master mix (Promega). All values were obtained in triplicates.

Primers for mouse samples are listed below:

TRF1-F 5'-GTCTCTGTGCCGAGCCTTC-3'

TRF1-R 5'-TCAATTGGTAAGCTGTAAGTCTGTG-3'

TBP1-F 5'-ACCCTTCACCAATGACTCCTATG-3'

TBP1-R 5'-TGACTGCAGCAAATCGCTTGG-3'

PCR

DNA from frozen tissue samples was extracted using Phenol:Chloroform:Isoamyl:Alcohol (Sigma). Cre-mediated recombination by PCR was determined using the following primers:

F: 5′-ATAGTGATCAAAATGTGGTCCTGGG-3′

R: 5′-GCTTGCCAAATTGGGTTGG-3′

125

126 **Quantification and statistical analysis**

127 Survival data were analyzed by Kaplan Meier survival curves, and comparisons
128 were performed by *Log Rank* test. Statistical analysis was performed using GraphPad
129 Prism 5.03. Comparison of the percentage of mice in Figures 3, 4, 5, 7 and 8 was
130 performed by *Chi-Square* test.

131 Immunofluorescence quantifications were performed with Definiens software
132 and immunohistochemistry quantifications were performed by direct cell counting.
133 *Unpaired Student's t test* was used to determine statistical significance. P values of
134 less than 0.05 were considered significant. Statistical analysis was performed using
135 Microsoft® Excel 2011.

136
137

References

Jacks, T., Remington, L., Williams, B. O., Schmitt, E. M., Halachmi, S., Bronson, R. T. and Weinberg, R. A. (1994) 'Tumor spectrum analysis in p53-mutant mice', *Current Biology*, 4(1), pp. 1–7. doi: 10.1016/S0960-9822(00)00002-6.

Martínez, P., Thanasoula, M., Muñoz, P., Liao, C., Tejera, A., McNees, C., Flores, J. M., Fernández-Capetillo, O., Tarsounas, M. and Blasco, M. A. (2009) 'Increased telomere fragility and fusions resulting from TRF1 deficiency lead to degenerative pathologies and increased cancer in mice', *Genes and Development*, 23(17), pp. 2060–2075. doi: 10.1101/gad.543509.

Ruzankina, Y., Pinzon-Guzman, C., Asare, A., Ong, T., Pontano, L., Cotsarelis, G., Zediak, V. P., Velez, M., Bhandoola, A. and Brown, E. J. (2007) 'Deletion of the Developmentally Essential Gene ATR in Adult Mice Leads to Age-Related Phenotypes and Stem Cell Loss', *Cell Stem Cell*, 1(1), pp. 113–126. doi: 10.1016/j.stem.2007.03.002.

Serrano, M., Lee, H. W., Chin, L., Cordon-Cardo, C., Beach, D. and DePinho, R. A. (1996) 'Role of the INK4a locus in tumor suppression and cell mortality', *Cell*, 85(1), pp. 27–37. doi: 10.1016/S0092-8674(00)81079-X.